

Analysis Of Modified Surface Topographies Of Titanium-Based Hip Implants Using Finite Element Method

Aleksandra Vulović^{1,2*}, Fernando Gustavo Warchomicka³, Florian Pixner³, Nenad Filipović^{1,2}

¹ Faculty of Engineering, University of Kragujevac, Sestre Janjic 6, 34000 Kragujevac, Serbia

² Bioengineering Research and Development Center, Prvoslava Stojanovica 6, 34000 Kragujevac, Serbia

³ Institute of Materials Science, Joining and Forming, Graz University of Technology, Kopernikusgasse 24/1, A-8010 Graz, Austria

*corresponding author

Abstract:

BACKGROUND:

In order to ensure the proper function of the cementless hip implant, the connection between the femoral bone and the implant has to be as strong as possible. According to experimental studies, implants with a rough surface reduce micro-movements between femoral bone and implant, which helps form a stronger connection between them.

OBJECTIVE:

The goal of this study was to analyze how half-cylinder surface topographies of different diameter values affect shear stress values and their distribution on the surface of the hip implant and trabecular femoral bone.

METHODS:

Nine models with different half-cylinder diameter values (200 μ m, 400 μ m, and 500 μ m) and distances between half-cylinders were created for the analysis using the finite element method. Each model consisted of three layers: implant, trabecular, and cortical femoral bone.

RESULTS:

For all three diameter values, the highest shear stress value, for the implant layer, was located after the first half-cylinder on the side where force was defined. For the trabecular bone, the first half-cylinder was under lower amounts of shear stress.

CONCLUSION:

If we only consider shear stress values, we can say that models with 400 μ m and 500 μ m diameter values are a better choice than models with 100 μ m diameter values.

Keywords: Finite Element Analysis, Hip Implant, Shear Stress,

Surface Topography

1. Introduction

Average life expectancy has significantly increased in the past decades. As a result of aging, we are faced with a variety of health challenges. Some of those challenges, such as arthritis, lead to chronic hip pain and can significantly reduce mobility. In those situations, the hip replacement procedure is necessary to improve the quality of life. Total hip arthroplasty (THA) is considered one of the most successful surgeries in terms of mobility improvement and pain relief. During this procedure, both femoral bone and cartilage are replaced with an artificial stem and cup. Several types of implant fixation are being used, while the most common ones are cemented and cementless. The best type of fixation, for different parameters, has been a topic of discussion for a long time [1-4]. The disadvantages of cementless hip implants compared to cemented ones are longer healing time, price, unsuitability for older age, and possible complications such as stress shielding and thigh pain. On the other side, the advantages of cementless hip implants include the lower amount of time required to perform THA and easier fixation [3]. Cementless implants depend on the body's ability to form a strong connection with the implant, known as osseointegration, which also means that one of the main reasons for revision procedure is related to the aseptic loosening of the bone-implant connection. During the past decades, experimental work presented information about how the osseointegration process can be improved by the design of the implants, including their surface properties, as well as with bone-implant interface factors [5].

The properties on the surface of the implant are important for the biological system response towards implant. It has influence on the bone cell behaviour and thus the connection between bone and implant. Surface modifications of the implants should retain the mechanical and physical properties of the initial material while at the same time improving the surface properties that can influence the forming of the bone implant connection [6]. Modification techniques allow us to increase the implant's surface roughness in order to improve its biocompatibility. The first approach to analyzing implant surfaces was using in vivo experiments. The majority of the published studies are related to oral implants which are under different loading conditions than orthopedic implants. The experimental studies related to dental implants indicate that better bone-implant integration can be achieved by increased surface roughness [7-9] and stronger bone response [10]. It was also shown that not all modification techniques provide the same results [11].

An increasing number of implant surface modifications have been created without knowing if one surface modification will provide better results than others. Comparative studies using various implant surfaces are rarely performed, which is why we decided to undertake this task. To the best of our knowledge, there is no large-scale numerical study dedicated to the effect of hip implant topographies on the shear stress distribution. Many factors can have an impact on bone response and implant fixation (e.g. immunological response), however, we solely considered surface topographies. The technique of surface modification and surface chemistry were out of the scope

of the present work. For the numerical analysis of the models, the Finite Element Analysis has been utilized. This approach has been used for decades for a variety of problems, from analyzing constructions to applying it in biomedical engineering. Inside the field of biomedical engineering, it found application in many segments including the research focused on skeletal systems and implants, such as dental implants [12,13], knee implants [14,15], and hip implants [16,17,18,19]. Nowadays, numerical analysis is being used in combination with experiments to provide more insights regarding different surface topographies.

Based on the performed studies, we know that porous implants are a better choice compared to solid implants in terms of forming a stronger bone-implant connection. When evaluating porous implants, a few parameters should be considered: porosity, pore size, pore interconnectivity, and pore geometry [5]. In this paper, we focused on two parameters – pore geometry and pore size. Although there is not only one appropriate pore size, it is known that it should be at least 100 μm which allows for the necessary surface area in order to achieve cell adhesion and as a result increase the load-bearing capacity [20]. The effect of pore shape on the osseointegration process is not well known as with other parameters. Based on the research by Chang et al. [21] cylindrical pores have shown the best results in terms of strength, and osteoconductivity. However, there are a lot of unknowns related to the size and shape of pores. Our aim with the paper is to contribute to this field by performing a number of studies using the finite element method in

order to assess the surface shear stress which is known to affect bone-implant connection.

We have analyzed 9 models that will be presented in section 2. So far, there have not been performed analyses of so many different implant modifications and that is the contribution of this paper to this field of research. The presented results include shear stress distribution as it is considered to be an important parameter for aseptic loosening. With this study, we wanted to analyze how different shapes of surface modification change the shear stress distribution and values. Based on that we performed the comparative analysis to choose the modification that could potentially be the best choice for a hip implant.

2. Materials & Methods

2.1 Geometries

Each developed model consisted of three layers – the hip implant layer, the femoral cortical bone layer, and the femoral trabecular bone layer. For the model development, we used computer-aided design (CAD) software and exported each layer as a .stp file. The dimensions of the models based on the implant and bone dimensions are presented in Figure 1. We used three different half-cylinder diameters and three different distances between them to represent different implant surface topographies.

Figure 1. Model dimensions

The created models are based on realistic geometry and they capture the essential features of the bone-implant interface. The shape of topography and the values based on previous studies and literature review, presented in section 1. Three diameter values of half-cylinders were considered - 200 μm , 400 μm , and 500 μm . The diameter values were selected to match the pore size values that are shown to achieve cell adhesion, which is necessary for achieving better connection between the femoral bone and the implant.

In order to investigate the effect of different distance values between half-cylinders on the shear stress distribution, three scenarios for each diameter value were considered. The distance values were either equal to the diameter, two times the diameter, or three times the diameter. We chose this parameter as a variable to better understand how it influences the shear stress distribution along the bone-implant interface, which is an important factor for implant stability and osseointegration.

A total of nine models were created. The model depth was 1mm and the total length was 50mm or 100mm depending on the diameter value. In order to reduce the required computation power, the size of the model for a diameter value of 200 μm was reduced in terms of length. Instead of 100mm, the length for the models with 200 μm diameter was 50mm as the analysis of models with 400 μm and 500 μm showed that the biggest change in the results is noticeable in the first half of the model.

Each model had distinct hip implant surface topography in the shape of half-cylinders. Trabecular femoral bone layers were modeled to follow the shape of the implant topographies. An example of implant and trabecular femoral layer is shown in Figure 2.

Figure 2. Example of contact between the implant and trabecular femoral layer

For each model, mesh was manually created. We scaled up the models by 10 times to facilitate the meshing and analysis process. A mesh dependency study was conducted, and it was shown that elements size corresponding to two times the radius value gave results that had a 5% result difference compared to much finer mesh (three times more elements). Element size and total element numbers are presented in Table 1. The first number in the table corresponds to the diameter value, while the second one corresponds to the distance between half-cylinders.

Table 1. Element size and total element numbers for each model

Element size for cortical femoral bone was higher compared to the other two layers and it was 5mm.

2.2 Material Properties and Boundary Conditions

Three materials were considered – titanium alloy (Ti6Al4V) which is commonly used for cementless hip implants and femoral trabecular and cortical bone. All materials were considered to be isotropic with Young's modulus of elasticity and Poisson's coefficient values

adapted from literature [22-24]. Although material properties of cortical and trabecular bone are anisotropic, it was shown that in the case of static loading bone that corresponds to single-leg standing, bone properties can be considered isotropic [25]. The values of the considered material properties are shown in Table 2.

Table 2. Applied Young's modulus of elasticity and Poisson's coefficient

For the simulations, the upper surface of the cortical femoral bone was fixed while the bottom surface of the implant was locked in the z-direction. Additionally, the side surfaces of both bones and implant were locked in the x-direction. The force was defined on the surface of the implant in order to simulate the implant being pushed out. A value of 1000N was defined on the whole implant surface. Figure 3 shows the applied boundary conditions.

Figure 3. Applied boundary conditions

Only static load was considered in this paper as the goal was to filter out the best topographies before moving to more complex loading. Dynamic loads will be considered in our future studies. In order to include micro motions that can occur between cortical bone and implant, linear contact with friction between femoral trabecular bone and implant was defined. We have applied the friction coefficient of 0.39, obtained from the literature [23]. Additionally, the connection

between cortical and trabecular femoral bone was considered as glued contact. All analyses were performed using NX Nastran 11.4.1.

3. Results and Discussion

3.1 Diameter 200 μ m

The obtained shear stress values were the highest for the models with 200 μ m diameter. Shear stress distribution for the implant and trabecular bone are presented in Figures 4 and 5. As can be noticed for both layers, a higher distance between half-cylinders corresponds to a higher maximum shear stress value increase. For the implant layer, the maximum value was located after the first half-cylinder on the side where force was defined.

Figure 4. Implant shear stress distribution for 200 μ m diameter

Figure 5. Trabecular bone shear stress distribution for 200 μ m diameter

For the trabecular layer, the maximum values were located on the half-cylinders surfaces located in the middle of the models. The first and the last half-cylinder on the trabecular bone model had the lowest shear stress values.

Table 3. Comparison of results for 200 μ m diameter

The implant maximum shear stress values were between 9 - 18% higher compared to trabecular bone shear stress values. The lowest difference was noticed for model 200_200, and it was calculated to

be 9.44%. Differences for the other two models were in a similar range – 17.59% for model 200_400 and 15.57% for model 200_600.

3.2 Diameter 400 μ m

The obtained shear stress values for 400 μ m diameter were significantly lower compared to values obtained for 200 μ m diameter values. Shear stress distribution for the implant and trabecular bone are presented in Figures 6 and 7. Again, the increasing distance between half-cylinders leads to a higher maximum shear stress value. The maximum value was located after the first half-cylinder on the side where force was defined.

Figure 6. Implant shear stress distribution for 400 μ m diameter

For the trabecular layer, high were located on almost all of the half-cylinders surfaces. The last half-cylinder on the trabecular bone model had the lowest shear stress values for two of of three cases (distance 400 μ m and 800 μ m). As can be noticed on the bottom model in Figure 7, the first half-cylinder surface had the lowest shear stress values.

Figure 7. Trabecular bone shear stress distribution for 400 μ m diameter

Table 4. Comparison of results for 400 μ m diameter

The implant maximum shear stress values were between 12 - 17% higher compared to trabecular bone shear stress values. The lowest

difference was noticed for model 400_400, and it was calculated to be 12.45%. Differences for the other two models were in a similar range – 16.31% for model 400_800 and 16.57% for model 400_800.

3.3 Diameter 500 μ m

The obtained shear stress values for the last considered diameter of 500 μ m showed similar results to those presented for 400 μ m diameter. Shear stress distribution for the implant and trabecular bone are presented in Figures 8 and 9. Again, the increasing distance between half-cylinders leads to a higher maximum shear stress value. The maximum value was located after the first half-cylinder on the side where force was defined. It can be noticed that surface topographies in the middle model (distance 1000 μ m) in Figure 8, had higher shear stress values compared to other two models.

Figure 8. Implant shear stress distribution for 500 μ m diameter

Figure 9. Trabecular bone shear stress distribution for 500 μ m diameter

For the trabecular layer, similar situation was noticed as with the 400 μ m diameter. High shear stress values were located on almost all of the half-cylinders surfaces. The last half-cylinder on the trabecular bone model had the lowest shear stress values for all three cases. In two out of three cases (distance 1000 μ m and 1500 μ m), the first half-cylinder surface had lower shear stress values.

Table 5. Comparison of results for 500 μ m diameter

The implant maximum shear stress values were between 7 - 16% higher compared to trabecular bone shear stress values. The lowest difference was noticed for model 500_1000, and it was calculated to be 7.54%. Differences for the other two models were 12.38 % for model 500_500 and 15.06% for model 500_1500.

3.4 Comparison of the results

The mechanical aspect of the bone-implant connection is affected by shear stress. High shear stress can damage the bone-implant interface which affects the stability and longevity of the implant. In order to avoid that, shear stress should be reduced. For all three diameter values, the implant layer had the highest shear stress value after the first half-cylinder on the force-applied side. For the trabecular bone, the pattern was different, as the first half-cylinder topography had lower shear stress values than the rest. This should be taken into consideration when designing the implant geometry and surface topography.

The obtained results for all presented diameter values are consistent with our previous results for 4 μ m diameter, where it was also obtained that a smaller distance between half-cylinders results in lower shear stress values [26]. This indicates that the distance between the half-cylinders is an important factor to consider in order to reduce shear stress values. Additionally, we found that models with 200 μ m diameter had more than twice as high shear stress values compared to models with 400 μ m and 500 μ m diameter values. This is

in line with previous findings on dental implants [27] and it suggests that higher surface roughness can reduce shear stress in the implant. This implies that the diameter of the half-cylinders is another important factor for reducing shear stress.

4. Conclusion

Primary stability is essential for the long-term success of implant insertion. This stability means that the implant fits tightly in the bone and is able to resist movement which is achieved through the mechanical interlocking with bone tissue. There are a number of factors that can influence the primary stability of the inserted implant. One of those factors is related to implant surface topography, which was the focus of this paper.

In this paper, we investigated how different surface patterns of Ti-6Al-4V affect the shear stress distribution on the implant-bone interface using the Finite Element Method. Shear stress is one of the important parameters that influence the mechanical aspect of the bone-implant connection. High shear stress can cause damage or deformation to the bone-implant interface, and the aim is to reduce it as much as possible in order to achieve a better connection. By using the Finite Element Analysis, we can save time and analyze the effect of different surface topographies more efficiently. This also helps to narrow down the choices of surface topographies that require further *in vivo* testing.

In this study, we performed the analyses of 9 different models that had different half-cylinder diameters and different distances

between the half-cylinders. The half-cylinder diameters were 200 μm , 400 μm , and 500 μm , and the distances between them varied as well. We obtained the shear stress values for each model and found that the models with the smallest diameter (200 μm) had much higher maximum shear stress values than the models with the larger diameters (400 μm and 500 μm). Therefore, if we only consider the shear stress criterion, for the determination of the optimal surface topography, we can conclude that the models with larger diameters are more suitable choices. However, our results are based on static loading conditions and do not account for other factors such as fatigue, corrosion, bone quality, or biological response. These factors can affect the performance and longevity of hip implants *in vivo*. Moreover, our models are simplified and cannot completely capture the complexity of the bone-implant interface. And that is the main limitation of the presented study. Therefore, further studies are needed to validate our findings under dynamic conditions and to optimize the design of hip implant surfaces for better clinical outcomes. Additionally, more realistic and patient-specific models are needed to evaluate the effect of individual anatomical and biomechanical factors on shear stress distribution and bone remodeling around hip implants.

Acknowledgement

This research is supported by the project that has received funding from the European Union's Horizon 2020 research and innovation programmes under grant agreement No 952603 (SGABU project).

This article reflects only the authors' view. The Commission is not responsible for any use that may be made of the information it contains. A.V. and N.F. also acknowledge the funding by the Ministry of Science, Technological Development and Innovation of the Republic of Serbia, contract number [451-03-47/2023-01/200107 (Faculty of Engineering, University of Kragujevac)].

Conflict of interest

The authors declare that they have no conflict of interest.

References

- [1] Marinelli M, Soccetti A, Panfoli N, de Palma L. Cost-effectiveness of cemented versus cementless total hip arthroplasty. A Markov decision analysis based on implant cost. *Journal of Orthopaedics and Traumatology*. 2008; 9(1): p. 23-28.
- [2] Maggs J, Wilson M. The relative merits of cemented and uncemented prostheses in total hip arthroplasty. *Indian journal of orthopaedics*. 2017; 51(4): p. 377-385.
- [3] Zhang C, Yan CH, Zhang W. Cemented or cementless fixation for primary hip arthroplasty—evidence from The International Joint Replacement Registries. *Annals of Joint*. 2017; 2(10): p. 57.

- [4] Konan S, Abdel MP, Haddad FS. Cemented versus uncemented hip implant fixation: Should there be age thresholds? *Bone & Joint Research*. 2019; 8(12): p. 604-607.
- [5] Liu Y, Rath B, Tingart M, Eschweiler J. Role of implants surface modification in osseointegration: A systematic review. *Journal of Biomedical Materials Research Part A*. 2020; 108(3): p. 470-484.
- [6] Warchomicka F. Surface topographies on the micro and nanoscale of metal alloys for tissue regeneration. In *Nanostructured biomaterials for regenerative medicine.*: Woodhead Publishing; 2020. p. 315-336.
- [7] Cooper LF. A role for surface topography in creating and maintaining bone at titanium endosseous implants. *The Journal of prosthetic dentistry*. 2000; 84(5): p. 522-534.
- [8] Shalabi MM, Gortemaker A, Van't Hof MA, Jansen JA, Creugers N. Implant surface roughness and bone healing: a systematic review. *J Dent Res*. 2006; 85(6): p. 496-500.
- [9] Le Guéhennec L, Soueidan A, Layrolle P, Amouriq Y. Surface treatments of titanium dental implants for rapid osseointegration. *Dental materials*. 2007; 23(7): p. 844-854.
- [10] Wennerberg A, Albrektsson T. Effects of titanium surface topography on bone integration: a systematic review. *Clinical oral implants research*. 2009; 20: p. 172-184.

- [11] Uno M, M H, R O, J S, H I, T O. Mechanical Interlocking Capacity of Titanium with Respect to Surface Morphology and Topographical Parameters. *J Dent Oral Biol.* 2020; 5(2): p. 1163.
- [12] Bahuguna R, Anand B, Kumar D, Aeran H, Anand V, Gulati M. Evaluation of stress patterns in bone around dental implant for different abutment angulations under axial and oblique loading: A finite element analysis. *National journal of maxillofacial surgery.* 2013; 4(1): p. 46.
- [13] Zor, ZF., Kılınc, Y, Erkmén, E, Kurt, A. How do implant threads and diameters affect the all-on-four success? A 3D finite element analysis study. *Technology and Health Care.* 2022; 30(5), p. 1031-1042.
- [14] Godest AC, Beaugonin M, Haug E, Taylor M, Gregson PJ. Simulation of a knee joint replacement during a gait cycle using explicit finite element analysis. *Journal of biomechanics.* 2002; 35(2): p. 267-275.
- [15] Baldwin MA, Clary CW, Fitzpatrick CK, Deacy JS, Maletsky LP, Rullkoetter PJ. Dynamic finite element knee simulation for evaluation of knee replacement mechanics. *Journal of biomechanics.* 2012; 45(3): p. 474-483.
- [16] Bennett D, Goswami T. Finite element analysis of hip stem designs. *Materials & design.* 2008; 29(1): p. 45-60.
- [17] Katz Y, Lubovsky O, Yosibash Z. Patient-specific finite element analysis of femurs with cemented hip implants. *Clinical Biomechanics.* 2018; 58: p. 74-89.

- [18] Chethan KN, Zuber M, Shenoy S, Kini CR. Static structural analysis of different stem designs used in total hip arthroplasty using finite element method. *Heliyon*. 2019; 5(6): p. e01767.
- [19] Wang CC, Lee CH, Chin NC, Chen KH, Pan CC, Su KC. Biomechanical analysis of the treatment of intertrochanteric hip fracture with different lengths of dynamic hip screw side plates. *Technology and Health Care*. 2020;28(6): p. 593-602.
- [20] Zaharin HA, Abdul Rani AM, Azam FI, Ginta TL, Sallih N, Ahmad A, et al. Effect of unit cell type and pore size on porosity and mechanical behavior of additively manufactured Ti6Al4V scaffolds. *Materials*. 2018; 11(12): p. 2402.
- [21] Chang BS, Hong KS, Youn HJ, Ryu HS, Chung SS, Park KW. Osteoconduction at porous hydroxyapatite with various pore configurations. *Biomaterials*. 2000; 21(12): p. 1291-1298.
- [22] Soni A, Chawla A, Mukherjee S. Effect of muscle contraction on knee loading for a standing pedestrian in lateral impacts. In 20th ESV conference; 2007.
- [23] Das S, Sarangi SK. Finite Element Analysis of Femur Fracture Fixation Plates. *International Journal of Basic and Applied Biology*. 2014; 1(1): p. 1-5.
- [24] Aradhya KSS, Doddamani MR. Characterization of Mechanical Properties of SiC/Ti6Al-4V Metal Matrix Composite (MMC) Using Finite Element Method. *American Journal*. 2015; 5(3C): p. 7-11.

- [25] Peng L, Bai J, Zeng X, Zhou Y. Comparison of isotropic and orthotropic material property assignments on femoral finite element models under two loading conditions. *Medical engineering & physics*. 2006; 28(3): p. 227-233.
- [26] Vulović A, Filipović N. Computational analysis of hip implant surfaces. *J. Serb. Soc. Comput. Mech*. 2019; 13(1): p. 109-119.
- [27] Aunmeungtong W, Khongkhunthian P, Rungsiyakull P. Stress and strain distribution in three different mini dental implant designs using in implant retained overdenture: a finite element analysis study. *ORAL & implantology*. 2016; 9(4): p. 202.

TABLES

Table 1. Element size and total element numbers for each model

Model	Element size [mm]	Total element number	Model	Element size [mm]	Total element number	Model	Element size [mm]	Total element number
<i>200_200</i>	0.4	160930	<i>400_400</i>	0.8	90090	<i>500_500</i>	1	51840
<i>200_400</i>	0.4	157000	<i>400_800</i>	0.8	80190	<i>500_1000</i>	1	53110
<i>200_600</i>	0.4	157210	<i>400_1200</i>	0.8	84880	<i>500_1500</i>	1	55440

Table 2. Applied Young's modulus of elasticity and Poisson's coefficient

	Ti6Al4V	Cortical femoral bone	Trabecular femoral bone
<i>Young's modulus of elasticity [MPa]</i>	109000	16700	295
<i>Poisson's coefficient</i>	0.34	0.3	0.315

Table 3. Comparison of results for 200µm diameter

Model	Implant	Trabecular bone
	Maximum shear stress [MPa]	Maximum shear stress [MPa]
<i>200_200</i>	8.429	7.633
<i>200_400</i>	11.01	9.073
<i>200_600</i>	13.66	11.26

Table 4. Comparison of results for 400µm diameter

Model	Implant	Trabecular bone
	Maximum shear stress [MPa]	Maximum shear stress [MPa]
<i>400_400</i>	3.005	2.631
<i>400_800</i>	4.174	3.493
<i>400_1200</i>	5.43	4.53

Table 5. Comparison of results for 500 μ m diameter

Model	Implant	Trabecular bone
	Maximum shear stress [MPa]	Maximum shear stress [MPa]
<i>500_500</i>	2.957	2.591
<i>500_1000</i>	3.954	3.656
<i>500_1500</i>	5.378	4.568

FIGURE CAPTIONS

Figure 1. Model dimensions

Figure 2. Example of contact between the implant and trabecular femoral layer

Figure 3. Applied boundary conditions

Figure 4. Implant shear stress distribution for 200 μ m diameter

Figure 5. Trabecular bone shear stress distribution for 200 μ m diameter

Figure 6. Implant shear stress distribution for 400 μ m diameter

Figure 7. Trabecular bone shear stress distribution for 400 μ m diameter

Figure 8. Implant shear stress distribution for 500 μ m diameter

Figure 9. Trabecular bone shear stress distribution for 500 μ m diameter

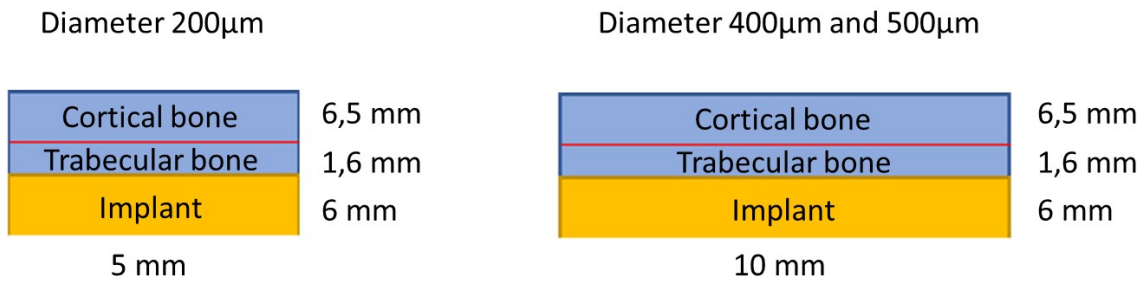
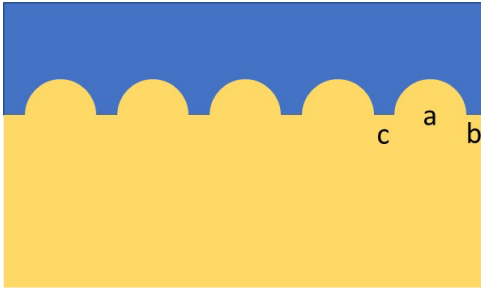


Figure 1. Model dimensions



Parameters:

a – diameter values (200 μ m, 400 μ m, 500 μ m)

b – distance from the edge where force is defined $b = 5 * a$

c – distance between half-cylinders

case 1: $c = a$

case 2: $c = 2 * a$

case 3: $c = 3 * a$

Figure 2. Example of contact between the implant and trabecular

femoral layer

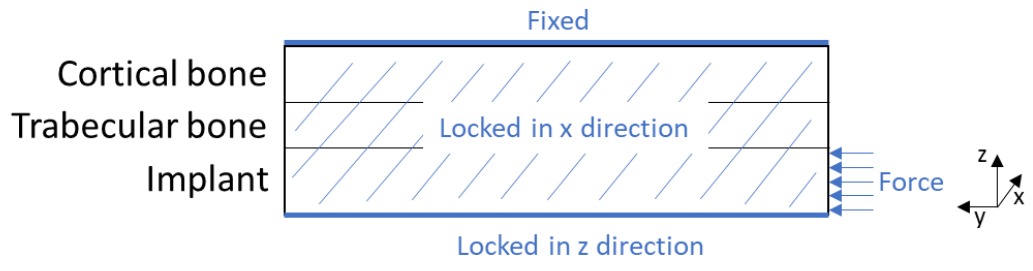


Figure 3. Applied boundary conditions

Implant models – diameter 200 μ m
Distance: 200 μ m; 400 μ m; 600 μ m

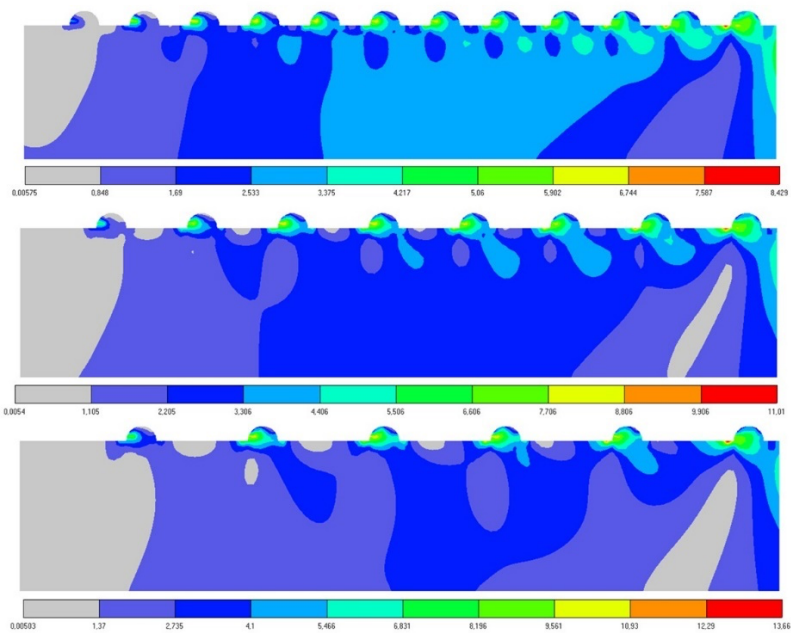


Figure 4. Implant shear stress distribution for 200 μ m diameter

Trabecular bone models – diameter 200 μ m
Distance: 200 μ m; 400 μ m; 600 μ m

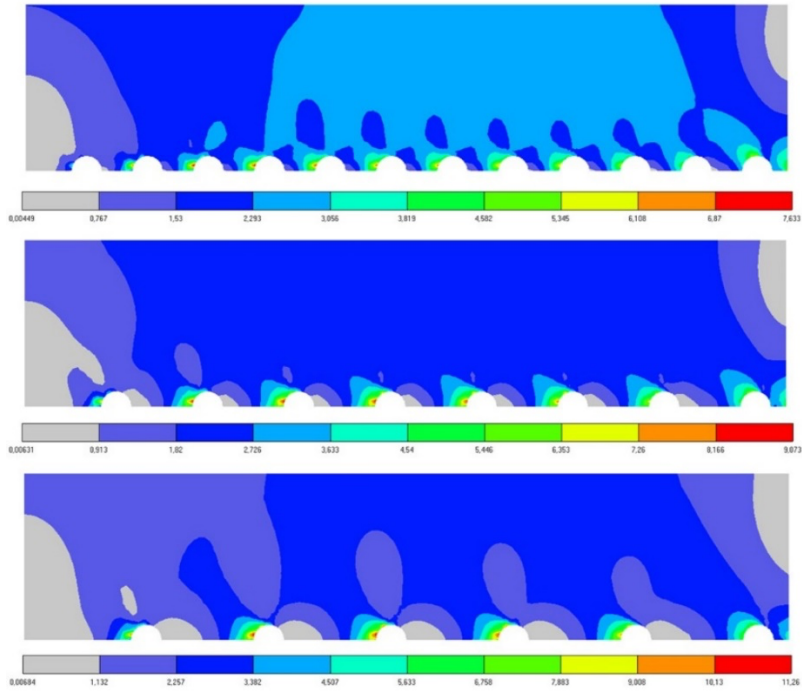


Figure 5. Trabecular bone shear stress distribution for 200 μ m diameter

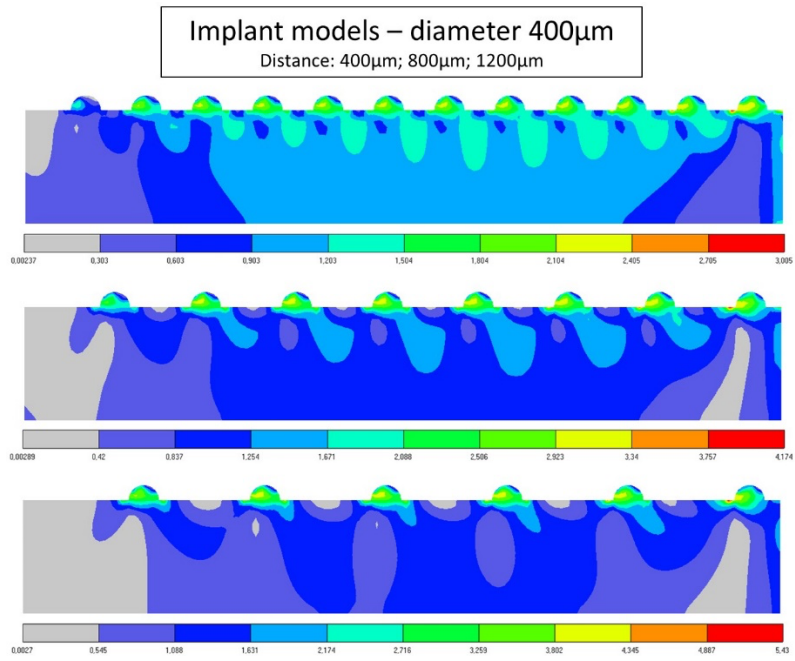


Figure 6. Implant shear stress distribution for 400 μ m diameter

Trabecular bone models – diameter 400 μ m
Distance: 400 μ m; 800 μ m; 1200 μ m

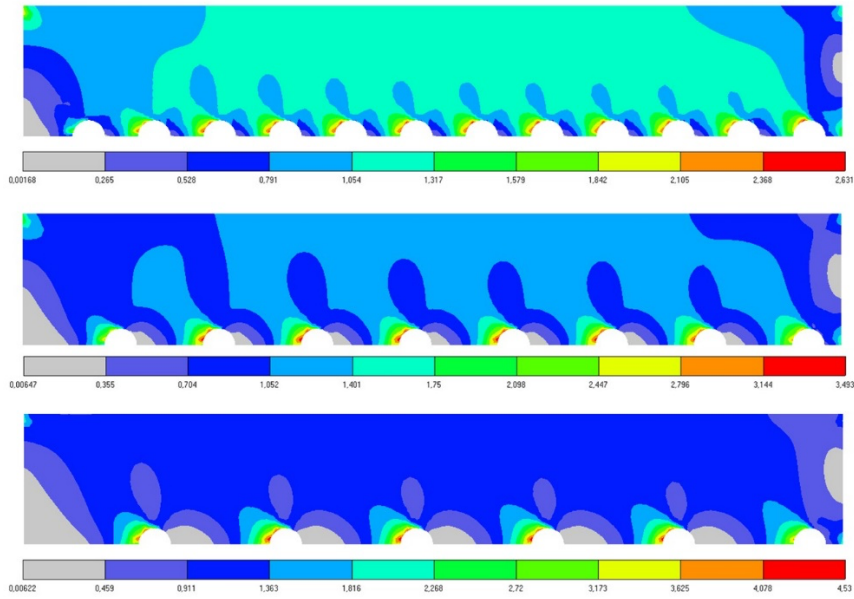


Figure 7. Trabecular bone shear stress distribution for 400 μ m diameter

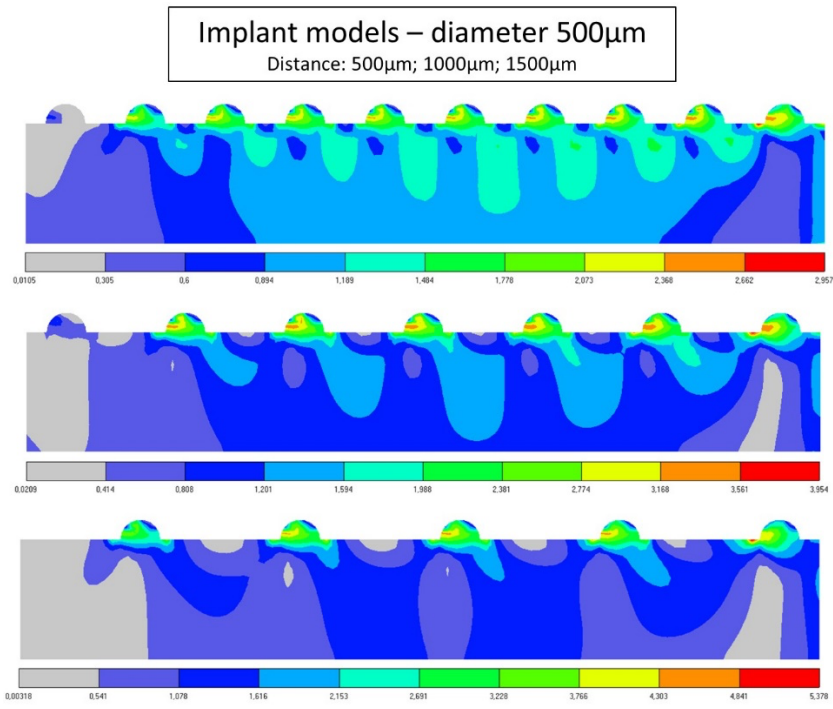


Figure 8. Implant shear stress distribution for 500 μ m diameter

Trabecular bone models – diameter 500 μ m
Distance: 500 μ m; 1000 μ m; 1500 μ m

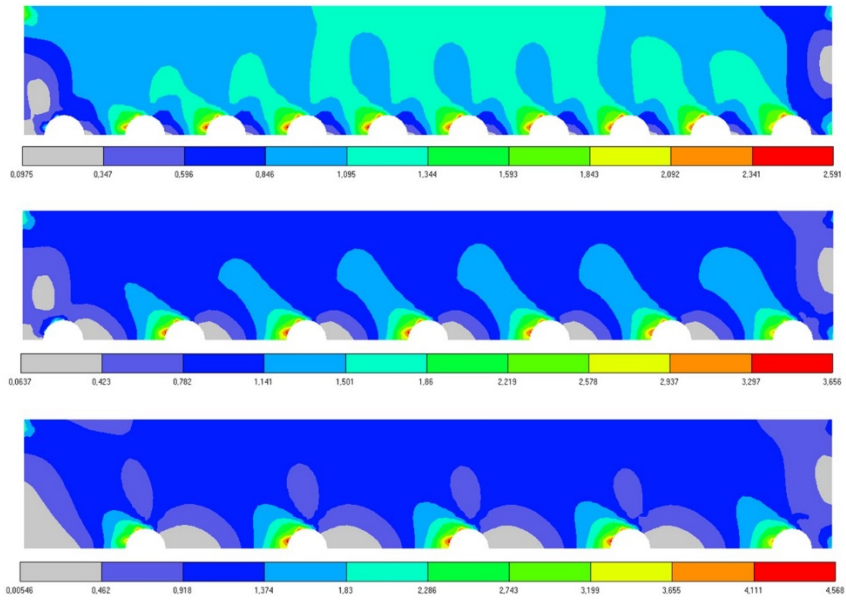


Figure 9. Trabecular bone shear stress distribution for 500 μ m diameter